EPJ Web of Conferences **123**, 03004 (2016) DOI: 10.1051/epjconf/201612303004
Heavy Ion Accelerator Symposium 2015

Probing cluster structures through sub-barrier transfer reactions

D. C. Rafferty[1,a], M. Dasgupta[1], D. J. Hinde[1], C. Simenel[1], E. C. Simpson[1], E. Williams[1], I. P. Carter[1], K. J. Cook[1], D. H. Luong[1], S. D. McNeil[1], K. Ramachandran[2], K. Vo-Phuoc[1], and A. Wakhle[3]

[1]*Department of Nuclear Physics, Australian National University, Canberra, Australia*
[2]*Nuclear Physics Division, Bhabha Atomic Research Centre, Mumbai, India*
[3]*National Superconducting Cyclotron Laboratory, Michigan State University, East Lansing, MI, USA*

Abstract. Multinucleon transfer probabilities and excitation energy distributions have been measured in ^{16,18}O, ^{19}F + ^{208}Pb at energies between 90% - 100% of the Coulomb barrier. A strong 2p2n enhancement is observed for all reactions, though most spectacularly in the ^{18}O induced reaction. Results are interpreted in terms of the Semiclassical model, which seems to suggest α-cluster transfer in all studied systems. The relation to cluster-states in the projectile is discussed, with the experimental results consistent with previous structure studies. Dissipation of energy in the collisions of ^{18}O is compared between different reaction modes, with cluster transfer associated with dissipation over a large number of internal states. Cluster transfer is shown to be a long range dissipation mechanism, which will inform the development of future models to treat these dynamic processes in reactions.

1 Introduction

The propensity of nucleons within the nuclear medium to coalesce into alpha- particles has been known since the earliest days of nuclear physics. Alpha-decay, in which the Helium nucleus emerges preformed from the parent nuclide was one of the first discoveries in the field. In fact, some of the initial models of nuclear structure (prior to the discovery of the neutron) posited the alpha particle as the basic building block of the nucleus [1]. Such models quickly fell out of favour with the formulation of the liquid drop and shell model of the nucleus, which were better able to predict nuclear properties. However, in recent years cluster models have seen a renaissance, due to their ability to predict certain peculiar spectral properties of some light nuclei.

A classic example of a cluster is the first excited 0^+ state in ^{12}C, known as the Hoyle state [2]; a resonance state of three alpha particles that decays only very rarely to stable ^{12}C, and is the sole production mechanism of this isotope, that is essential to all life on earth. Whilst many studies have examined the properties of cluster resonance states in α-conjugate nuclei (those that are even-even with N = Z), more recently cluster states have been identified in non-conjugate nuclei, with this phenomena seen to be particularly important in neutron-rich nuclei that have become accessible with the advent of radioactive ion beam facilities. The influence of such structures on reaction dynamics remains mostly unexplored.

Coupled channels models have been very successful at reproducing fusion cross sections in the near-barrier region [3], but there are discrepancies both above and far below where cross sections are hindered relative to the predictions [4, 5]. At above barrier energies this has been attributed to dissipative processes that occur during the very violent impact between the ions. Past experiments have shown that dissipation remains important even at sub-barrier energies, so may also have some bearing on the hindrance effects seen in this energy region. Cluster transfer is a possible long-range dissipation mechanism [6], since the cluster states that might be expected to participate are predicted to be radially diffuse [7].

In this work multi-nucleon transfer probabilities and excitation energy distributions in ^{16,18}O, ^{19}F + ^{208}Pb spanning the well-below to above barrier energy regions have been measured. The chosen projectiles have been previously identified to exhibit clustering properties in the context of structure studies [8]. How multi-nucleon transfer varies between the projectiles and how the prominence of different channels evolves as a function of the internuclear separation, as well as how energy is dissipated between the reaction partners has been studied.

2 Experiment

An experiment was performed at the Heavy Ion Accelerator facility at the ANU in June 2013, in which a ^{208}Pb target was bombarded with ^{16}O, ^{18}O, and ^{19}F beams, at energies from 100% to 90% of the Coulomb barrier V_B. The experimental setup is shown in Fig 1. The light projectile-like fragments were detected at 160.6^o, with yields normalized to elastic scattering events in two forward angle monitor detectors to obtain absolute transfer probabilities.

[a]e-mail: dominic.rafferty@anu.edu.au

The detector used in this experiment was a simple Frisch-grid ionization chamber, coupled to a Silicon detector [9]. As ions enter the detector, their energy loss in the gas (ΔE) is recorded together with their residual energy on reaching the Silicon detector ($E_{\rm Si}$). Together these allow a separation of the reaction products in mass and Z.

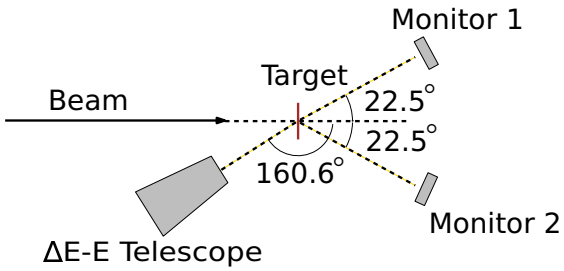

Figure 1. Schematic diagram of experimental setup.

3 Analysis

To identify reaction products, the unique locus of each species must be determined from the $\Delta E - E_{\rm Si}$ spectrum, a typical example of which is shown in Fig. 2(a). The red line in the figure shows the locus of ^{12}C, mapped by tracing the distribution of inelastically scattered ^{12}C from a thick tantalum target. Projecting the $\Delta E - E_{\rm Si}$ spectrum in ΔE allows for a separation of the products within the gated region shown in Fig. 2 by mass. A typical mass separation spectrum is shown in Fig. 2(b), where the products are rebinned according to their relative ΔE compared to a product for which the locus in the $\Delta E - E$ spectrum is well known.

4 Results

The measured transfer probabilities have been interpreted in terms of the Semiclassical model [10]. In this approach, the probability of each mode has the form:

$$P(r_{\rm min}) \propto \exp(-2\alpha r_{\rm min}) \quad (1)$$

Where $r_{\rm min}$ is the distance of closest approach, and α is related to the binding energy of the transfered nucleons. α can be calculated or extracted from transfer probability data, by fitting the exponential slope of the probabilities outside the barrier radius- for the systems studied, this involves fitting the data beyond $r_{min} \geq 13.2$ fm. At the sub-barrier energies studied, it is assumed that the trajectories are purely Coulomb enabling a calculation of $r_{\rm min}$ using:

$$r_{\rm min} = \frac{Z_p Z_t e^2}{4\pi\epsilon}\left(1 + \csc\frac{\theta_{\rm c.m}}{2}\right) \quad (2)$$

where p and t denote projectile and target respectively. In this simple model of independent sequential transfer, the probability for transfer of N nucleons is a simple product of probabilities:

$$P_{Nn} = (P_{1n})^N \quad (3)$$

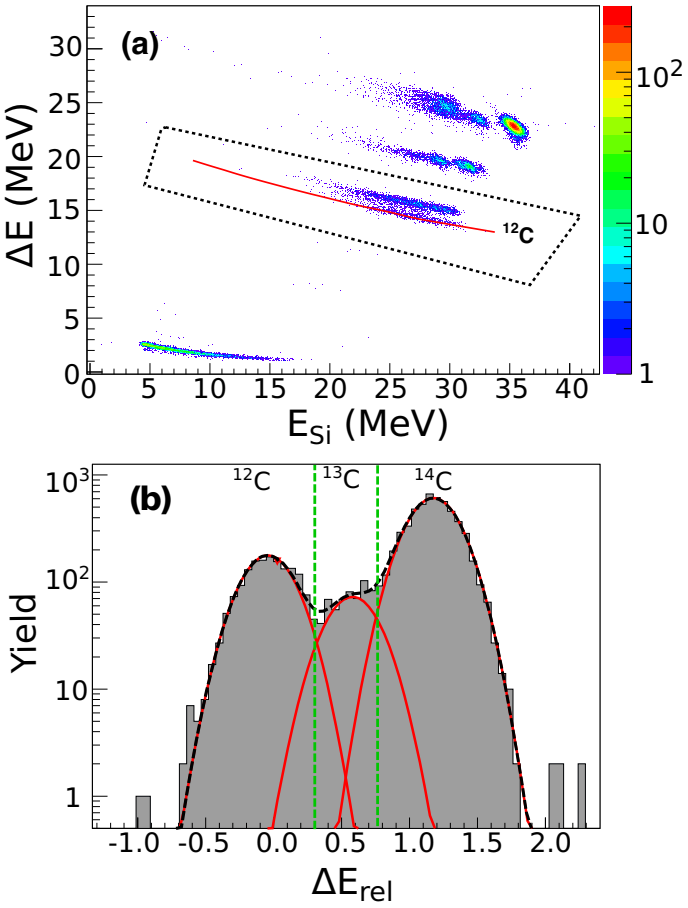

Figure 2. (Colour online) (a) $\Delta E - E_{\rm Si}$ plot obtained in the reaction ^{16}O + ^{208}Pb at 0.98V$_B$. The red line shows the ^{12}C locus from which the relative energy loss (ΔE_{rel}) spectrum is calculated. The ΔE_{rel} spectrum is determined from events within the dashed contour. (b) Resulting ΔE_{rel} spectrum. Black dashed curve shows the multiple Gaussian function fitted to the distribution. Red curves indicate the resulting fitted components, which are attributed to yields of the expected isotopes, in this case ^{12,13,14}C. Vertical dashed lines show the gate limits as determined by the intersections between adjacent fitted peaks.

More realistic transfer probabilities can be calculated with advanced microscopic models [11, 12]. In this section transfer probabilities as a function of $r_{\rm min}$ and an example of the extracted excitation energy spectra are shown.

4.1 Transfer Probabilties

4.1.1 $^{16}O + ^{208}Pb$: Fig. 3

Single proton transfer is shown to be dominant over the energy range considered. The semiclassical prediction for 2p transfer is shown as the red dashed line in this figure. This is the square of a fit to the 1p data beyond 13.2 fm, where the loss of flux to fusion does not disturb the exponential slope α. As shown, the two prominent $\Delta Z = 2$ modes shown in the figure are strongly enhanced relative to this prediction. Also interesting is the increasing equiv-

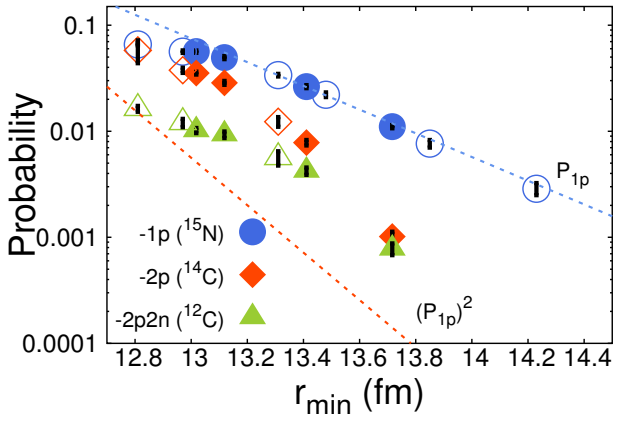

Figure 3. Transfer probabilities in ^{16}O + ^{208}Pb. Full symbols are the measurements reported from the June 2013 experiment. Empty symbols are those measured in a previous experiment [13] with a lower mass resolution. Blue dashed line shows a fit to the 1p data in the range r_{min} > 13.2 fm. Red dashed line shows the square of the fitted function, representing the prediction of the Semiclassical model for sequential transfer (see equation 2).

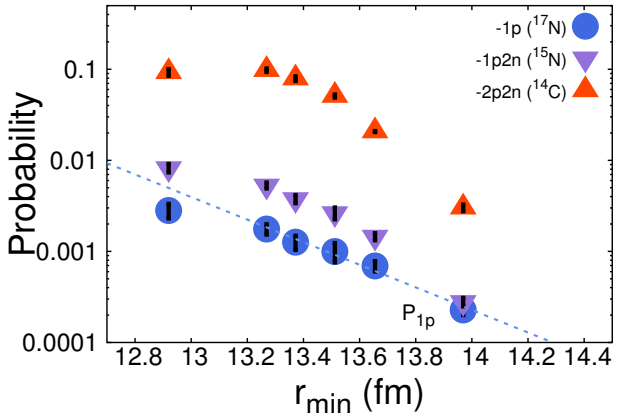

Figure 4. Transfer probabilities in ^{18}O + ^{208}Pb. Blue dashed line shows a fit to the 1p data in the range r_{min} > 13.2 fm.

alence of the 2p and 2p2n modes with increasing radial separation.

4.1.2 $^{18}O + ^{208}Pb$: Fig. 4

Single proton transfer is comparatively weak in this reaction. The transfer is dominated by 2p2n transfer over all distances, and also the 1p2n mode is far stronger than 1p, though these become equivalent at larger separations. Again shown is the fit of 1p data, but the semiclassical predictions (e.g. $P_{2p} = (P_{1p})^2$) for all other significant transfer modes in this case are not visible within the range of the figure.
Previous experiments have demonstrated a rich cluster structure in ^{18}O [8, 14, 15], with α resonant states found over a wide excitation range and attributed to a ^{14}C + α cluster structure. This is fully consistent with such a dominance of 2p2n over other transfer modes.

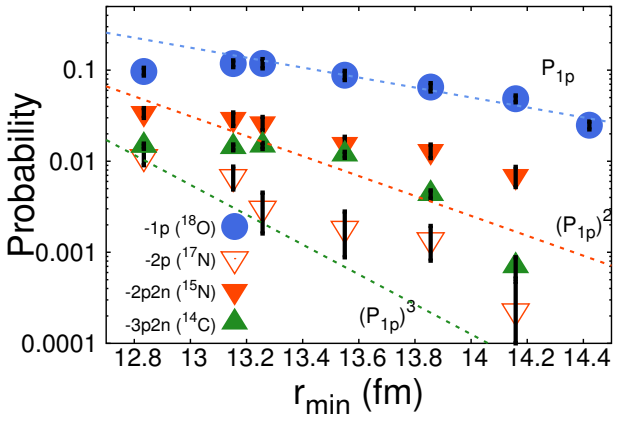

Figure 5. Transfer probabilities in ^{19}F + ^{208}Pb. Blue dashed line shows a fit to the 1p data in the range r_{min} > 13.2 fm. Red and green dashed lines are the square and cube respectively of the fitted 1p function, corresponding to the prediction of the semi-classical model (equation 2).

4.1.3 $^{19}F + ^{208}Pb$: Fig. 5

Single proton transfer is strongest here over the whole energy range. 2p is shown to be very weak, falling in fact lower than the Semiclassical prediction. ΔZ = 2 transfer is dominated by the 2p2n mode. A strong population of events with ΔZ = -3, with a significant yield of ^{14}C at all energies is observed. The 3p2n is most significant, and is equivalent in magnitude to 2p2n at higher energies. This channel falls off quickly however, whilst the 2p2n decays in proportion to 1p with increasing distance.
Previous studies of this reaction at energies closer to the barrier [16] found similar results, and interpreted this behaviour as evidence of clustering in ^{19}F, and in particular that the strong enhancement of 3p2n transfer was indicative of a direct (non-sequential) transfer of p + α. Here it is shown that this enhancement seems to disappear at larger internuclear separations. The strong 2p2n mode, on the other hand, seems to maintain the enhancement down to the deep sub-barrier region.

4.2 Energy Dissipation

The reaction Q-value is reconstructed on an event-by-event basis, from which the excitation energy can be derived. The Q-value can be determined from:

$$Q = \frac{A_3 + A_4}{A_4} E_3 - \frac{A_4 - A_1}{A_4} E_1 - \frac{2\sqrt{A_1 A_3 E_1 E_3}}{A_4} \cos\theta_{\text{lab}} \quad (4)$$

Where the subscript notation is in standard reaction form 1(2,3)4, with E denoting energies and A atomic masses. The excitation energy is then obtained from the difference between this value and the ground state Q-value for the reaction mode in question $Q_{g.g}$:

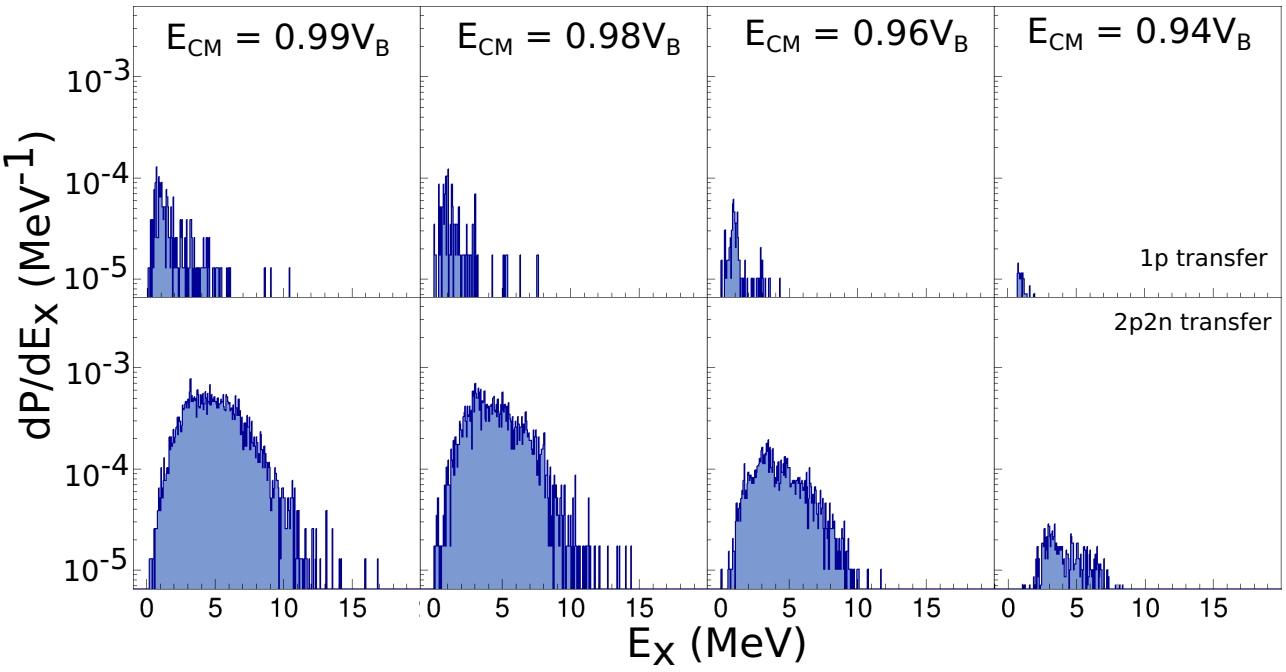

Figure 6. Excitation energy distribution of 1p and 2p2n modes in ^{18}O + ^{208}Pb as it varies with bombarding energy, given in units of the Coulomb barrier energy V_B.

$$E_x = Q_{g.g} - Q \quad (5)$$

In Fig. 6 shown is the recorded E_x spectra for the 1p and 2p2n transfer modes in ^{18}O + ^{208}Pb. Since the target is so much heavier, with a much higher level density than the light projectiles, the target-like fragment is expected to absorb most of the excitation energy in the transfer process. Observed in Fig. 6 is that whilst the transfer of a single proton shows a detailed structure most concentrated at low E_x, the transfer of 2p2n (α) is associated with a strong broad distribution of energy extending up to higher E_x distributions, reaching $\sim$ 10 MeV even at the lowest energy.

5 Conclusions

It has been demonstrated that there are vastly different transfer reactions between the ^{16,18}O, ^{19}F + ^{208}Pb. These effects are likely related to cluster structures that can be found in the projectiles. The very strong 2p2n transfer mode in ^{18}O + ^{208}Pb is consistent with previous investigations into clustering in ^{18}O. ^{16}O, despite being an α-conjugate nucleus, displays comparatively weak 2p2n transfer, though it appears to grow in relation to 2p with internuclear separation. ^{19}F also displays a strong 2p2n mode, that can be attributed to cluster transfer on the basis of the very weak 2p mode.

Excitation energy distributions involving the transfer of multiple nucleons are typically broad and featureless, and it has been shown how in ^{18}O + ^{208}Pb the transfer of an α-particle led to high excitation energies, well above the particle emission thresholds in the target-like fragment, even well below the barrier. While omitted here for brevity, ^{16}O and ^{19}F-induced reactions show similar behaviour. This is a potential mechanism through which energy dissipation can occur at long separations.

It is the goal of this project to establish the systematics of how this differs among light to medium mass projectiles, at energies near to far below the Coulomb barrier. A modified version of the coupled channels code CCFULL [17] is in development to incorporate dissipation into this framework in an attempt to understand the effect of dissipation on fusion cross sections.

Acknowledgements

Thanks go to all of the technical staff at the ANU heavy ion accelerator facility for their support. This work was supported by Australian Research Council grants FT120100760 and FL110100098.

References

[1] L. R. Hafstad and E. Teller, Phys. Rev. **54**, 681 (1938).
[2] F. Hoyle, The Astrophysical Journal Supplement Series **1**, 121 (1954).
[3] K. Hagino and N. Takigawa, Progress of theoretical physics **128**, 1001 (2012).
[4] J. O. Newton, R. D. Butt, M. Dasgupta *et al.*, Phys. Rev. C **70**, 024605 (2004).
[5] M. Dasgupta, D. Hinde, A. Diaz-Torres *et al.*, Physical review letters **99**, 192701 (2007).

[6] A. Diaz-Torres, D. Hinde, M. Dasgupta *et al.*, Physical Review C **78**, 064604 (2008).
[7] Y. Kanada-En'yo, M. Kimura and H. Horiuchi, Comptes rendus Physique **4**, 497 (2003).
[8] E. Johnson, G. Rogachev, V. Goldberg *et al.*, The European Physical Journal A **42**, 135 (2009).
[9] G. F. Knoll, *Radiation detection and measurement* (John Wiley & Sons, 2010)
[10] R. A. Broglia and A. Winther (1991).
[11] C. Simenel, Phys. Rev. Lett. **105**, 192701 (2010).
[12] G. Scamps and D. Lacroix, Phys. Rev. C **87**, 014605 (2013).
[13] M. Evers, M. Dasgupta, D. Hinde *et al.*, Physical Review C **84**, 054614 (2011).
[14] G. Morgan, D. Tilley, G. Mitchell *et al.*, Nuclear Physics A **148**, 480 (1970).
[15] V. Goldberg, K. M. Källman, T. Lönnroth *et al.*, Physics of Atomic Nuclei **68**, 1079 (2005).
[16] D. Biswas, R. Choudhury, B. Nayak *et al.*, Physical Review C **56**, 1926 (1997).
[17] K. Hagino, N. Rowley and A. Kruppa, Computer Physics Communications **123**, 143 (1999).